Structural, Magnetic, and Transport Properties of $R_xBa_{1-x}TiO_{3-\delta}$ Solid Solutions, Where R = La, Nd, Gd, Er, and Y: Rare-Earth-Dependent Metal-to-Semiconductor Transitions

Cahit Eylem,[†] Gotthård Sághi-Szabó,[†] Bai-Hao Chen,[†] Bryan Eichhorn,*[,†] Jian-Liang Peng,[‡] Richard Greene,*[,‡] Lourdes Salamanca-Riba,[§] and Sahn Nahm[§]

Center for Superconductivity Research and Departments of Chemistry and Biochemistry, Physics and Astronomy, and Materials and Nuclear Engineering, University of Maryland, College Park, Maryland 20742

Received March 9, 1992. Revised Manuscript Received June 26, 1992

Compositionally homogeneous solid solutions of formula $R_xBa_{1-x}TiO_{3-\delta}$ (where R = La, Nd; $0 \le x \le 1$) have been prepared by the dc arc-melting method. The La system showed a negative deviation from Vegard's Law due to BaO deficiencies, whereas the members of the Nd series were stoichiometric and showed a linear relationship between x and the lattice constant a. Limited substitution of the smaller rare earths Gd and Er were also achieved at low values of x (for Gd, $0 \le x \le 0.4$; Er, $0 \le x \le 0.3$) with virtually no substitution at high values of x. Single-phase oxygen deficient cubic $Y_xBa_{1-x}TiO_{3-\delta}$ phases were obtained (where $0 \le x \le 0.4$ and $0 < \delta \le 0.15$). Two compositionally dependent phase transitions occur in the La and Nd systems: tetragonal ($P4mm$)-to-cubic ($Pm3m$) at very low values of x (<0.05) which is second order and cubic ($Pm3m$)-to-orthorhombic ($Pbnm$) at high values of x which appears to be first order. HREM and electron diffraction studies showed no evidence for A-site ordering, microdomain ordering, or superstructure formation in the cubic regions. The single-phase samples disproportionate into $BaTiO_3$ and $R_2Ti_2O_7$ phases upon heating to 1000 °C in air with the exception of $La_{0.33}Ba_{0.67}TiO_3$, which remains cubic upon oxidation with only a 0.8% increase in cell volume. Four-probe resistivity measurements showed metallic conductivities for a majority of the samples between R_{300} and 4 K with $R_{300} \approx 10^{-2}$–10^{-4} Ω·cm. Metallic conductivity correlates with the perovskite tolerance factor [$t = (r_A + r_O)/\sqrt{2}(r_B + r_O)$] and occurs when $0.93 < t < 1.02$ with semiconducting or insulating behavior occurring outside this range. Dc susceptibility studies showed large Pauli susceptibilities associated with the metallic samples with a correlation between the magnitude of the susceptibility and the number of d electrons. Superconductivity was not observed above 4 K in any of the samples. The effective magnetic moments of the Nd^{3+} ions in the $Nd_xBa_{1-x}TiO_3$ phases (ca. 3.3 μ_B) for $x \le 0.9$ were close to the free ion value (3.62 μ_B). Electron localization is discussed in terms of structural parameters and electronic effects.

Introduction

The rare-earth titanium(III) oxides $RTiO_3$ (where R = La to Yb and Y) represent a remarkable series of isostructural perovskites that are now well understood in terms of their crystal chemistry and properties.[1,2] All members of this series are isoelectronic (Ti^{3+}, d^1) and isostructural (perovskite-related $GdFeO_3$ structure type), yet the magnetic and transport properties vary dramatically with the size and electronegativity of the rare-earth ions.[2] For example, $LaTiO_3$ is a metal (or semimetal) at room temperature and a semiconductor at low temperatures with weak antiferromagnetic ordering. In contrast, $YTiO_3$ is a room-temperature semiconductor with a 0.22-eV bandgap and displays ferromagnetic ordering.[2]

The interest in these and other d^1 oxides has intensified recently due to the novel properties associated with these materials. Some of the early transition metal oxides are low-temperature superconductors, such as $LiTi_2O_4$,[3] $SrTiO_{3-x}$,[4] and Li_xNbO_2,[5] with critical temperatures ranging from 0.8 to 11.5 K. We are interested in preparing series of perovskite-related phases in which the carrier concentration can be adjusted to approach a d^1 electronic configuration. One such series is the solid solutions of $BaTiO_3$ [Ti^{4+}] with $RTiO_3$ [Ti^{3+}] (where R = rare-earth ion) in which the oxidation state of Ti can be systematically varied between +3 (d^1) and +4 (d^0). These compounds would be structurally and compositionally related to the 1–2–3 family of copper oxide superconductors but would possess an inverse electronic configuration. Preliminary investigations of the lanthanum systems, $La_xBa_{1-x}TiO_3$ and La/Sr/Ti/O, were reported several years ago,[6] but thorough studies of magnetic, structural, and transport properties associated with these materials were not performed. More recent studies on the R/Sr/Ti/O systems (R = La, Ce)[7a-c] have revealed substantial metallic regions in the $La_xSr_{1-x}TiO_3$ solid solutions and a new *Ibmm* structure[7a] for compounds with $0.20 < x < 0.7$. We have been investigating the structural, magnetic, and transport properties of $BaTiO_3$ solid solutions with various metallic and nonmetallic $RTiO_3$ phases (R = trivalent ion) in an attempt to understand the correlations between structure and properties of the materials. We report here the synthesis and properties of the $R_xBa_{1-x}TiO_{3-\delta}$ series, where R = La, Nd, Gd, Er, and Y. These compounds display rare-earth-dependent metal-to-semiconductor transitions

[†] Chemistry and Biochemistry.
[‡] Physics and Astronomy.
[§] Materials and Nuclear Engineering.

(1) MacLean, D. A.; Ng, H.-N.; Greedan, J. E. *J. Solid State Chem.* **1979**, *30*, 35.
(2) Greedan, J. E. *J. Less Common Met.* **1985**, *111*, 335.
(3) Johnston, D. C.; Prakash, H.; Zachariasen, W. H.; Viswanathan, R. *Mater. Res. Bull.* **1973**, *8*, 777.
(4) Koonce, C. S.; Cohen, M. L.; Schooley, J. F.; Hosler, W. R.; Pfeiffer, E. R. *Phys. Rev.* **1967**, *163*, 380.
(5) Geselbracht, M. J.; Richardson, T. J.; Stacey, A. M. *Nature* **1990**, *324*-326.
(6) (a) Johnston, W. D.; Sestrich, D. *J. Inorg. Nucl. Chem.* **1961**, *20*, 32. (b) Kestigian, M.; Ward, R. *J. Am. Chem. Soc.* **1954**, *76*, 6027.
(7) (a) Sunstrom, J. E., IV; Kauzlarich, S. M.; Klavins, P. *Chem. Mater.* **1992**, *4*, 346. (b) Sunstrom, J. E., IV; Kauzlarich, S. M.; Klavins, P. NIST Special Publication 804; *Proceedings of the International Conference of the Chemistry of Electronic Ceramic Materials*; Davies, P. K., Roth, R. S., Eds.; NIST: Washington, DC, 1991; p 217. (c) Kauzlarich, S. M., results to be published. (d) Sunstrom, J. E., IV; Kauzlarich, S. M. *Better Ceramics Through Chemistry*; *Proceedings of the Spring 1992 Materials Research Society Meeting*, in press.

0897-4756/92/2804-1038$03.00/0

Table I. Atomic Absorption and Thermogravimetric Analyses of the $R_xBa_{1-x}TiO_{3-\delta}$ Phases

compound	% Ba[a]	% Ti[a]	% O uptake[b]
$Nd_{0.33}Ba_{0.67}TiO_3$	39.7 (38.7)	19.5 (20.5)	1.0 (1.1)
$Nd_{0.7}Ba_{0.3}TiO_3$	18.4 (17.3)	19.7 (20.1)	2.3 (2.4)
$Nd_{0.85}Ba_{0.15}TiO_3$	8.7 (8.6)	19.3 (20.0)	2.7 (2.8)
$Nd_{0.9}Ba_{0.1}TiO_3$	5.4 (5.7)	20.7 (20.0)	2.9 (3.0)
$La_{0.33}Ba_{0.67}TiO_3$	39.9 (39.0)	20.7 (20.6)	1.1 (1.1)
$La_{0.6}Ba_{0.3}TiO_{2.9}$	19.6 (18.8)	20.9 (21.9)	2.1 (2.2)
$La_{0.7}Ba_{0.2}TiO_{2.9}$	12.8 (12.5)	21.7 (21.9)	2.6 (2.6)
$La_{0.85}Ba_{0.15}TiO_3$	8.6 (8.8)	19.8 (20.4)	2.8 (2.9)
$Y_{0.2}Ba_{0.8}TiO_{2.85}$	48.9 (49.7)	21.0 (21.7)	1.8 (1.8)
$Y_{0.33}Ba_{0.67}TiO_{2.9}$	42.1 (42.3)	22.1 (22.4)	1.9 (1.9)
$Y_{0.4}Ba_{0.6}TiO_{2.9}$	41.2 (38.8)	23.3 (22.6)	2.2 (2.3)

[a] Weight percent determined by flame atomic absorption spectroscopy. Theoretical percentages are given in parentheses. [b] Weight percent oxygen uptake as determined by thermogravimetric analysis. Theoretical percentages are given in parentheses.

that correlate with the perovskite tolerance factor, t, but are seemingly independent of the carrier concentrations. Concurrent studies[7d] on the La–Ba–Ti–O system by Kauzlarich and co-workers are quite similar to our results described herein.

Experimental Section

Sample Preparation. All starting materials were high-purity compounds (≥99.9%) purchased from CERAC. Rare-earth oxides (R_2O_3) were prefired at 1000 °C prior to use. All other reagents were used as received.

Stoichiometric ratios of $BaTiO_3$, R_2O_3, anatase-TiO_2, and Ti were intimately ground and pressed into pellets. Pelletized mixtures were then melted in a dc arc furnace purged with gettered Ar (UHP) which was further purified by melting a Zr button immediately prior to reaction. The system was evacuated and purged with Ar gas several times before the reaction. Samples were fired several times with repetitive turnings. The resulting phases were then pulverized in a percussion mortar, finely ground, and analyzed by powder X-ray diffraction (XRD). In some cases, it was necessary to refire the mixtures several times with intermediate regrindings to achieve single phase products. The compounds were brittle and gray–black to black in color.

Alternatively, high-temperature furnaces were used for sample preparation in some cases. Stochiometric proportions of ground and well-mixed oxides $BaTiO_3$, R_2O_3, TiO_2, and Ti were pelletized and loaded into alumina boats. The boats were then inserted into a vacuum-tight mullite tube system. The system was evacuated and backfilled with gettered Ar gas several times. The samples were heated at 1400 °C for 6 h, cooled to room temperature over 8 h, and characterized by XRD. Regrindings and refirings were often necessary to obtain single-phase materials.

All single-phase materials were stored in a Vacuum Atmospheres Co. drybox to prevent oxidation.

Sample Characterization. X-ray diffraction data were collected at 25 °C on a modified Phillips XRG 2000 diffractometer (Cu Kα radiation) interfaced with a RADIX databox and MDI software system. Cell refinement calculations were performed on all data collected between $20° \le 2\theta \le 60°$, which was corrected for sample displacement and zero-point error.

Titanium oxidation states were determined by thermogravimetric analysis (TGA). Large samples (100–150 mg) were loaded into platinum boats and heated in air at 1000 °C for 6 h, resulting in white powders. The weight gain upon oxidation was measured at room temperature by assuming that the final oxidation state of Ti was +4. Each sample was analyzed twice, and the average percent weight gain is reported in Table I.

Atomic absorption data were recorded on a Perkin-Elmer 2380 atomic absorption spectrometer. Analyses were performed on bulk single-phase samples that were initially dispersed in a lithium borate flux ($LiBO_2$) and then dissolved in dilute HNO_3 (5%). Ba and Ti contents were measured in duplicate, and the average determinations are listed in Table I.

Property Measurements. Magnetic susceptibilities of the $Nd_xBa_{1-x}TiO_3$ compounds were carried out on finely ground powders of single-phase samples by using a Quantum Design superconducting quantum interface (SQUID) magnetometer at applied fields of 10–50 000 Oe. Powdered samples were loaded into gelatin capsules for analysis, or alternatively, sintered pellets were suspended in the magnetic field by dental floss. The background magnetization of the empty capsules was measured and shown to be negligible in all cases. The magnetic susceptibilities of the $R_xBa_{1-x}TiO_{3-\delta}$ compounds (R = La, Y) were measured on single-phase sintered pellets that were suspended in the magnet by dental floss. All samples were screened for superconductivity by low-field dc susceptibility down to 4 K.

Resistivity measurements were conducted on arc-melted pellets by using a standard four-probe technique. Leads were attached by sputtering ca. 300–500 Å of Ti followed by ca. 300–500 Å of Au onto masked samples that were briefly cleaned in an Ar plasma immediately prior to sputtering. Insulated copper wires were then attached to the sputtered Au/Ti contacts with silver paste, and the samples annealed under 5% H_2 in Ar at 180 °C for 12 h. The resistances were measured between 4 and 298 K by using a standard four-probe resistivity apparatus. Contact resistances were determined to be much less than 1 Ω in all cases and did not vary significantly with temperature.

Electron diffraction (ED) and high-resolution transmission electron microscopic (HREM) studies were conducted on a JEOL 2000-FXII transmission electron microscope operated at 200 kV. The microscope specifications are spherical aberration coefficient $C_s = 2.3$ mm, chromatic aberration coefficient $C_c = 2.2$ mm, lattice resolution of 0.14 nm, and point image resolution of 0.28 nm. All lattice images were obtained using axial illumination. The samples for HREM studies were prepared from freshly synthesized $R_xBa_{1-x}TiO_3$ materials which were cut with a knife to obtain a fresh surface. During this process, several small crystals were obtained from the new surface and were placed between two copper folding grids for HREM observation.

Results

Synthesis and Properties. Perovskite phases of general formula $R_xBa_{1-x}TiO_{3-\delta}$ were prepared in which single-phase members were obtained for R = La, Nd ($0 \le x \le 1$); Gd ($0 \le x \le 0.2$), and Y ($0 \le x \le 0.4$). All samples were prepared by the dc arc melting method or in high-temperature furnaces. The phases prepared at 1400 °C in high-temperature furnaces were indistinguishable from the arc-melted samples of the same composition. The compounds are grey-black to black in color with the darker colors being associated with higher Ti^{3+} content. When ground into powders, the compounds slowly oxidize in air at room temperature. Due to the forcing conditions associated with the arc-melting procedure, the composition and lattice parameters of all phases prepared in this study were closely monitored (see Tables I and II). Each compound was prepared at least twice, and the lattice parameters were refined. Slight adjustments in composition resulted in slight but reproducible variations in lattice parameters and the appearance of impurity phases when compositions were off stoichiometry. We have found the arc-melting procedure to be both highly reproducible and controllable in the synthesis of the $R_xBa_{1-x}TiO_{3-\delta}$ phases.

$NdTiO_3$ and $LaTiO_3$ form extensive substitutional solid solutions with $BaTiO_3$ ($R_xBa_{1-x}TiO_{3-\delta}$ where R = Nd, La) throughout the range of composition $0 \le x \le 1$. Minor BaO impurities were detected in the stoichiometric La materials when $0.5 \le x \le 0.8$. The range of solid solution formation decreased as a function of size in the rare-earth ion from La to Er as shown in Figure 1. The refined cell parameters are listed in Table II. With the exception of the lanthanum series, the $R_xBa_{1-x}TiO_{3-\delta}$ phases are not amenable to changes in oxygen content (i.e., there is a fixed δ for a given R and x combination). Compositions prepared with excess oxygen result in the formation of $R_2Ti_2O_7$ impurities, whereas compositions deficient in oxygen produce $RTiO_3$ and $BaTiO_{3-\delta}$ impurities. The

Table II. Structural Data and Perovskite Tolerance Factors for the $R_xBa_{1-x}TiO_{3-\delta}$ Phases

system	cell parameters			struct[a]	t[b]
	a	b	c		
$BaTiO_3$	3.994 (3)		4.022 (3)	T	1.06
$La_{0.15}Ba_{0.85}TiO_3$	3.985 (2)			C	1.04
$La_{0.2}Ba_{0.8}TiO_3$	3.984 (1)			C	1.04
$La_{0.33}Ba_{0.67}TiO_3$	3.976 (2)			C	1.02
$La_{0.4}Ba_{0.6}TiO_3$	3.965 (2)			C	1.01
$La_{0.5}Ba_{0.4}TiO_{2.9}$	3.955 (2)			C	1.00
$La_{0.6}Ba_{0.3}TiO_{2.9}$	3.954 (2)			C	0.98
$La_{0.7}Ba_{0.2}TiO_{2.9}$	3.944 (2)			C	0.97
$La_{0.85}Ba_{0.15}TiO_3$	5.598 (4)	5.601 (6)	7.918 (8)	O	0.96
$La_{0.9}Ba_{0.1}TiO_3$	5.592 (2)	5.592 (3)	7.914 (6)	O	0.95
$LaTiO_3$	5.585 (1)	5.593 (2)	7.907 (5)	O	0.94
$Nd_{0.1}Ba_{0.9}TiO_3$	3.979 (3)			C	1.05
$Nd_{0.28}Ba_{0.72}TiO_3$	3.964 (1)			C	1.02
$Nd_{0.3}Ba_{0.7}TiO_3$	3.958 (2)			C	1.02
$Nd_{0.33}Ba_{0.67}TiO_3$	3.962 (5)			C	1.01
$Nd_{0.4}Ba_{0.6}TiO_3$	3.957 (1)			C	1.00
$Nd_{0.5}Ba_{0.5}TiO_3$	3.942 (1)			C	0.99
$Nd_{0.6}Ba_{0.4}TiO_3$	3.935 (1)			C	0.97
$Nd_{0.7}Ba_{0.3}TiO_3$	5.541 (7)	5.553 (7)	7.839 (9)	O	0.96
$Nd_{0.75}Ba_{0.25}TiO_3$	5.531 (6)	5.558 (6)	7.807 (8)	O	0.95
$Nd_{0.85}Ba_{0.15}TiO_3$	5.527 (6)	5.562 (6)	7.809 (8)	O	0.93
$Nd_{0.9}Ba_{0.1}TiO_3$	5.529 (6)	5.591 (6)	7.786 (8)	O	0.93
$Nd_{0.98}Ba_{0.02}TiO_3$	5.516 (4)	5.616 (3)	7.798 (4)	O	0.92
$NdTiO_3$	5.509 (5)	5.617 (5)	7.772 (6)	O	0.91
$Gd_{0.2}Ba_{0.8}TiO_3$	3.984 (6)			C	1.03
$Gd_{0.3}Ba_{0.7}TiO_3$[c]	3.961 (2)			C	1.01
$Gd_{0.33}Ba_{0.67}TiO_3$[c]	3.958 (4)			C	1.01
$Gd_{0.4}Ba_{0.6}TiO_3$[c]	3.946 (4)			C	
$Y_{0.2}Ba_{0.8}TiO_{2.85}$	3.992 (1)			C	1.02
$Y_{0.33}Ba_{0.67}TiO_{2.9}$	3.965 (1)			C	1.00
$Y_{0.4}Ba_{0.6}TiO_{2.9}$	3.962 (4)			C	0.98
$Er_{0.1}Ba_{0.9}TiO_3$[c]	3.985 (4)			C	
$Er_{0.3}Ba_{0.7}TiO_3$[c]	3.972 (2)			C	

[a] T = tetragonal, space group *P4mm*; C = cubic, space group *Pm3m*; O = orthorhombic, space group *Pbnm*. [b] Perovskite tolerance factor $t = (r_A + r_O)/\sqrt{2}(r_B + r_O)$ were calculated using Shannon's radii.[20] Twelve-coordinate radii for Y^{3+} were estimated based on the standard 11% increase from nine-coordinate radii for other rare-earth ions. Vacancies were not included in calculating average radii values. [c] Impurity lines present.

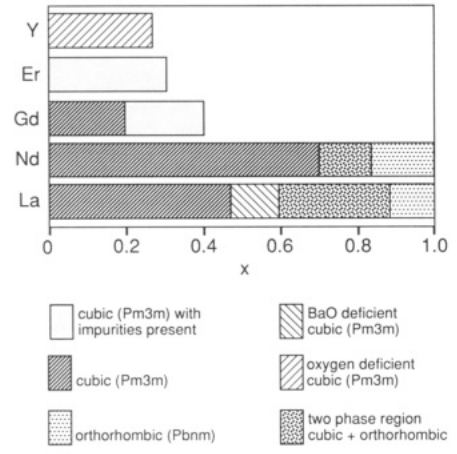

Figure 1. Structural phase diagram for the $R_xBa_{1-x}TiO_{3-\delta}$ series.

$Nd_xBa_{1-x}TiO_3$ series was well behaved with an extensive cubic region that rigorously obeyed Vegard's law. For this reason, the Nd series will be described first.

Several members of the $Nd_xBa_{1-x}TiO_3$ solid solution were prepared between $0 \le x \le 1.0$, and their cell parameters plotted as a function of x (see Figure 2a). A stacked plot of the XRD profiles for the $x = 0$, 0.33, 0.7, 0.9, and 1.0 are shown in Figure 3. $Nd_xBa_{1-x}TiO_3$ phases adopt the tetragonal $BaTiO_3$ perovskite structure (space group *P4mm*) when $x < 0.05$ and cubic symmetry (space group

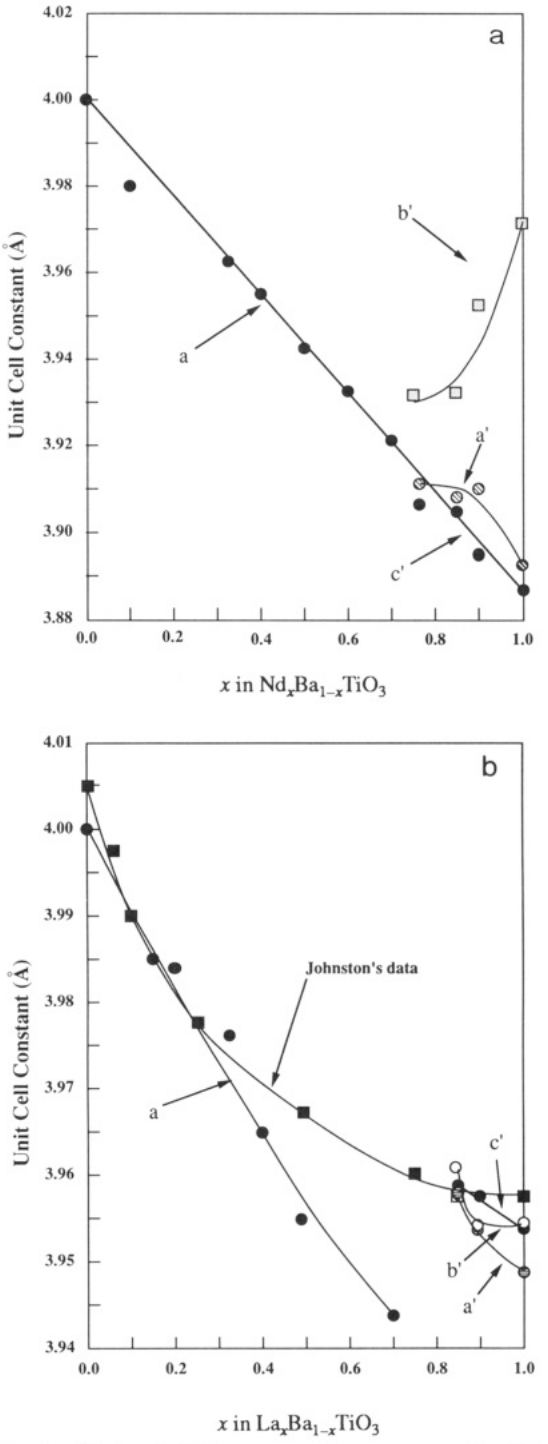

Figure 2. Plots of lattice parameter versus x for (a) the $Nd_xBa_{1-x}TiO_3$ series and (b) the $La_xBa_{1-x}TiO_3$ series. Johnstons's data is taken from ref 6a and is represented by the black squares. For $BaTiO_3$, the a parameter was obtained from $V^{1/3}$. In the orthorhombic regions, $a' = a_0/\sqrt{2}$, $b' = b_0/\sqrt{2}$ and $c' = c_0/2$.

Pm3m) at $x \ge \sim 0.05$. The cubic region persists from $0.05 < x \le 0.7$ and rigorously obeys Vegard's law. At $x \approx 0.7$, the system enters a biphasic region containing both the cubic and orthorhombic phases. At certain compositions between $0.7 \le x \le 0.85$, reflections for both the cubic and orthorhombic phases were observed. Beyond $x = 0.85$, single-phase orthorhombic solid solutions (space group *Pbnm*) are formed (Figure 3d). The existence of the biphasic region is best illustrated by monitoring the changes of the a and b unit cell parameters of the orthorhombic phases as they approach to cubic region (Figure 2a). As the cubic region is approached from the right, the a pa-

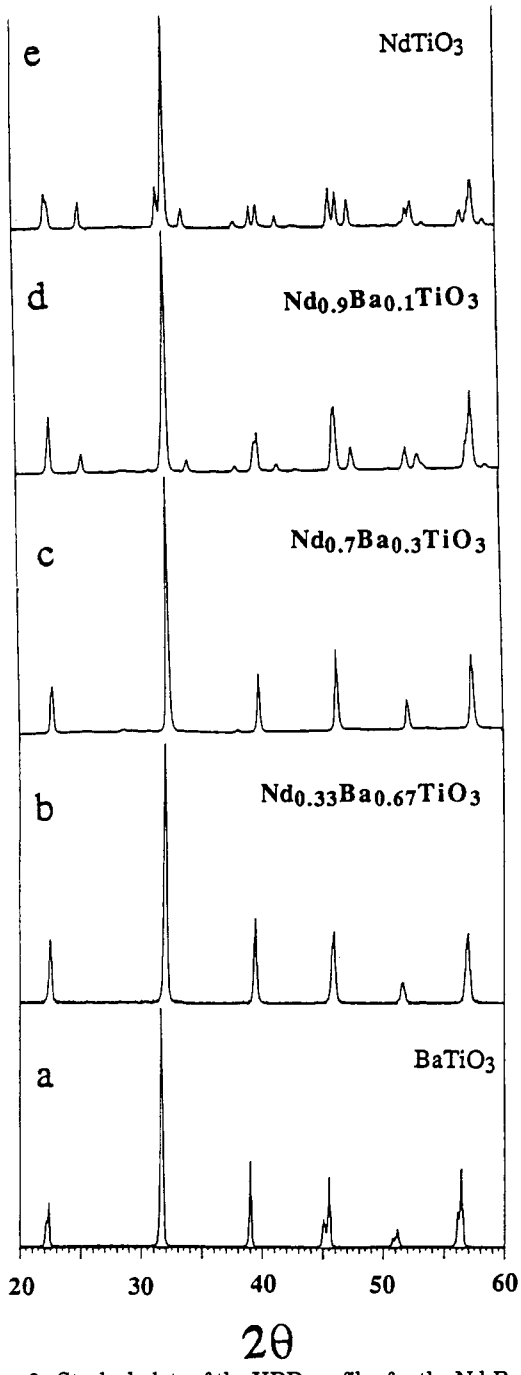

Figure 3. Stacked plots of the XRD profiles for the $Nd_xBa_{1-x}TiO_3$ series where $x = 0$ (a), $x = 0.33$ (b), $x = 0.7$ (c), $x = 0.9$ (d), and $x = 1.0$ (e).

rameter diverges from b, revealing the presence of the biphasic region which is suggestive of a first-order phase transition. Due to the nature of sample preparation (a 30-s quench from >2000 °C), the observed symmetry changes may not represent equilibrium conditions. Annealing the samples under Ar at 1400 °C and slow cooling to room temperature do not significantly affect the appearance of the XRD profiles.

The $La_xBa_{1-x}TiO_3$ system, previously studied by Johnston et al.,[6] was reported to contain single-phase samples over the range of composition $0 \leq x \leq 1$ with a large cubic region between $0 < x \leq 0.9$ that showed a significant negative deviation from Vegard's law. Our results are in qualitative agreement with their findings. A plot of the cell parameters as a function of x for our work and that of Johnston is shown in Figure 2b for comparison. The analytical data and refined cell parameters are given in Tables I and II, respectively. We repeatedly observed BaO impurities (ca. 5–10%) in the region $0.5 \leq x \leq 0.8$ which were not reported in the earlier studies.[6] Samples prepared with slight BaO deficiencies in the $0.5 \leq x < 0.6$ region resulted in the cubic single phases (Figure 1) which have smaller unit cell constants than the corresponding compounds prepared from stoichiometric mixtures. Samples prepared with slight BaO deficiencies in the $0.6 \leq x \leq 0.8$ region yielded both orthorhombic and cubic phases (see below) but without BaO impurities. The BaO deficiencies may be responsible for the negative deviation from Vegard's law in the cubic region. Attempts to introduce oxygen and barium vacancies independently resulted in the appearance of $BaTiO_{3-\delta}$ and other impurities.

There appears to be a biphasic region between $0.60 \leq x < 0.9$, but the X-ray data are not sufficiently accurate to illustrate the presence of both cubic and orthorhombic phases (see Figure 2b). However, electron diffraction and HREM studies on $La_{0.7}Ba_{0.2}TiO_{2.9}$ showed the coexistence of cubic ($a = a_p$) and orthorhombic ($a \approx b \approx \sqrt{2}a_p$, $c \approx 2a_p$) phases which confirms the biphasic nature of the sample. These experiments are discussed in the next section.

$GdTiO_3$ forms single-phase solid solutions with $BaTiO_3$ over the range of composition $0 \leq x \leq 0.2$ (Figure 1). $Gd_2Ti_2O_7$ pyrochlore appears as an impurity beyond $x = 0.2$; however, refinements of the cubic reflections between $0.2 < x \leq 0.4$ show that the unit cell continues to contract, suggesting that substitution is still occurring (Table II). Beyond $x = 0.4$, multiphase mixtures containing cubic $Gd_xBa_{1-x}TiO_3$, $GdTiO_3$, and $Gd_2Ti_2O_7$ were observed with no additional Ba for Gd substitution taking place. Attempts to make BaO and oxygen deficient phases in the region of $0.2 < x \leq 0.4$ did not result in any single-phase samples.

$YTiO_3$ and $ErTiO_3$ do not form stoichiometric solid solutions with $BaTiO_3$, yielding instead biphasic mixtures of $R_2Ti_2O_7$ pyrochlores and cubic Ba/R/Ti/O phases (R = Y, Er). As in the Gd system, cell refinements of the cubic phases in the biphasic mixtures (Table II) reveal that substitution is occurring between $0 \leq x \leq 0.4$ for R = Y and $0 \leq x \leq 0.3$ for R = Er. Introducing oxygen vacancies in the $Y_xBa_{1-x}TiO_3$ phases ($Y_xBa_{1-x}TiO_{3-\delta}$) resulted in single-phase cubic perovskites over the range $0 \leq x \leq 0.4$ (see Figure 1 and Table I) with δ varying from 0.10 to 0.15. As with the other $R_xBa_{1-x}TiO_{3-\delta}$ phases, there appears to be a fixed δ for each x and, in the case of the yttrium phases, the larger values of δ are associated with compositions having smaller x values. Oxidation of the $Y_xBa_{1-x}TiO_{3-\delta}$ phases in air at 1000 °C resulted in disproportionation to $Y_2Ti_2O_7$ and $BaTiO_3$. Substitution of Ba into the orthorhombic $RTiO_3$ was not observed for R = Gd, Er, Y.

The compounds are susceptible to slow oxidation at room temperature and are fully oxidized (white powders, Ti^{4+}) in ca. 2 h at 1000 °C in air. Except for the lanthanum series, the $R_xBa_{1-x}TiO_{3-\delta}$ compounds cleanly disproportionate to $R_2Ti_2O_7$ pyrochlores (or $La_2Ti_2O_7$ type phases) and $BaTiO_3$ upon oxidation. Interestingly, the $La_xBa_{1-x}TiO_3$ phases, where $0.1 \leq x \leq 0.33$, remain cubic upon oxidation (Figure 4) forming $La_xBa_{1-x}TiO_{3+x/2}$ single-phase materials in which a 0.8% increase in cell volume was observed for the $x = 0.33$ end member. Previous studies on the $La_xBa_{1-x}TiO_{3+x/2}$ system where $0 \leq x \leq 0.2$ by Toefield and Scott[8] showed that $La_{0.2}Ba_{0.8}TiO_{3.10}$ [Ti^{4+}]

(8) Tofield, B. C.; Scott, W. R. *J. Solid State Chem.* **1974**, *10*, 183.

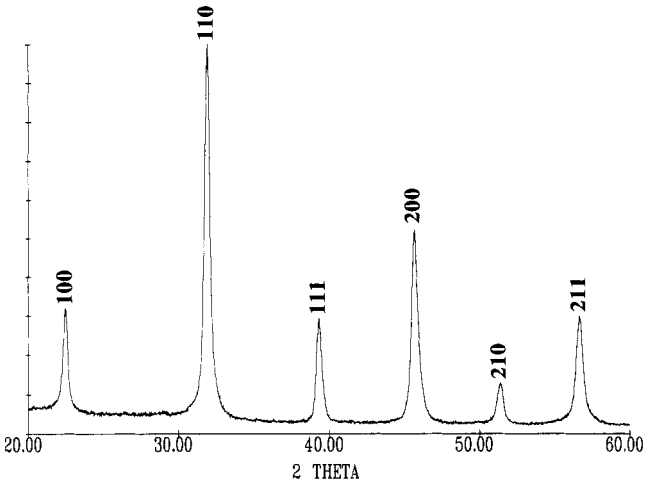

Figure 4. Indexed XRD profile of $La_{0.33}Ba_{0.67}TiO_{3.167}$ obtained from oxidizing $La_{0.33}Ba_{0.67}TiO_3$.

could be prepared only by firing the precursors in air, followed by reduction in H_2, and then refiring in air. This behavior seems inconsistent with proposed structural models involving interstitial oxygen atoms and suggests that significant A and B site defects may be present in the $La_xBa_{1-x}TiO_{3+x/2}$ phases in analogy to "$LaMnO_{3.1}$".[8] Repeated attempts to prepare $La_{0.33}Ba_{0.67}TiO_{3.167}$ directly from $BaCO_3$, TiO_2, and La_2O_3 resulted in a Ba/La/Ti/O cubic compound and other Ba/La/Ti/O phases.[9] Oxidation of the $La_xBa_{1-x}TiO_3$ phases where $0.33 < x \leq 1.0$ resulted in multiphase mixtures comprising $La_2Ti_2O_7$, cubic La/Ba/Ti/O, and other fully oxidized materials.

Structural Considerations. The phases in the cubic regions of the $R_xBa_{1-x}TiO_{3-\delta}$ series adopt the prototypical perovskite structure (space group *Pm3m*) with complete disordering of the Ba^{2+} and R^{3+} ions over the A sites. Annealing the samples at 1000 °C in Ar did not induce any detectable A site ordering or changes in lattice parameters. The lack of ordering of the R^{3+}/Ba^{2+} ions was verified by electron diffraction (ED) and HREM studies on several cubic samples. For example, electron diffraction studies of several $Y_{0.33}Ba_{0.67}TiO_{2.9}$ crystallites in several different zone axes clearly showed only the expected cubic reflections with lattice parameters in excellent agreement with the refined XRD data. The ED pattern and HREM image of the ⟨100⟩ zone of $Y_{0.33}Ba_{0.67}TiO_{2.9}$ (Figure 5a) shows the regular perovskite (100) spacings at 3.94 Å, which again is in good agreement with the refined cell parameter from the XRD experiments (3.965 (1) Å). As previously mentioned, the $Y_xBa_{1-x}TiO_{3-\delta}$ compounds cleanly phase separate to $BaTiO_3$ and $Y_2Ti_2O_7$ upon oxidation; thus, the absence of these phases in the HREM and ED experiments clearly indicate that the perovskite phases were not oxidized during sample preparation.

Electron diffraction and HREM studies on $La_{0.7}Ba_{0.2}TiO_{2.9}$ also showed the cubic perovskite phase with the expected lattice parameters (Figure 5b). In addition, a second phase was also identified (Figure 5c) which could be indexed on a primitive cubic cell with $a \approx 2a_p$ or on a primitive orthorhombic cell similar to that of $LaTiO_3$ ($a \approx b \approx \sqrt{2}a_p$, $c \approx 2a_p$). A similar problem of determining the correct crystal system and space group has historically been observed with $LaTiO_3$.[1,10] Careful examination of the orthorhombic reflections in the $0.6 \leq x \leq 0.8$ region of the $La_xBa_{0.9-x}TiO_{2.9}$ (10% BaO deficient) phases show that the (113) and (023) reflections always accompany the (013) reflection. Thus, an *I*-centered cell, such as the *Ibmm* cell observed in the $La_xSr_{1-x}TiO_3$ system,[7a] is apparently not formed. Under different synthetic conditions, an *Ibmm* structure may indeed be stabilized.[7d]

The structures of the $x = 0.33$ members of the $R_xBa_{1-x}TiO_{3-\delta}$ phases are of interest in that they are disordered compositional analogs of the 1–2–3 superconductors. The differences between the two structures reside in the absence of oxygen defects and A site ordering in the titanium phases. However, the general heavy atom positions and normalized cell dimensions are quite similar (the average perovskite related subcell in $YBa_2Cu_3O_7$ is 3.87 Å versus 3.97 Å for $Y_{0.33}Ba_{0.67}TiO_{2.9}$), yet no A site ordering in any of the titanium phases have been detected to date.

Table III. Conductivity Data for the $R_xBa_{1-x}TiO_{3-\delta}$ Phases

sample	transport behavior	approx resistivity at 298 K, Ω·cm	d electrons per formula unit
$La_{0.2}Ba_{0.8}TiO_3$	SC	0.4	0.20
$La_{0.33}Ba_{0.67}TiO_3$	M	0.05	0.33
$La_{0.4}Ba_{0.6}TiO_3$	M	0.008	0.40
$La_{0.5}Ba_{0.4}TiO_{2.9}$	M	0.003	0.50
$La_{0.6}Ba_{0.3}TiO_{2.9}$	M	0.001	0.60
$La_{0.7}Ba_{0.2}TiO_{2.9}$	M	0.005	0.70
$La_{0.85}Ba_{0.15}TiO_3$	M	0.0002	0.85
$Nd_{0.28}Ba_{0.72}TiO_3$	SC	0.1	0.28
$Nd_{0.33}Ba_{0.67}TiO_3$	M	0.005	0.33
$Nd_{0.4}Ba_{0.6}TiO_3$	M	0.008	0.40
$Nd_{0.5}Ba_{0.5}TiO_3$	M	0.08	0.50
$Nd_{0.6}Ba_{0.4}TiO_3$	M	0.002	0.60
$Nd_{0.7}Ba_{0.3}TiO_3$	M	0.002	0.70
$Nd_{0.85}Ba_{0.15}TiO_3$	M	0.002	0.85
$Nd_{0.9}Ba_{0.1}TiO_3$	M	0.01	0.90
$Nd_{0.98}Ba_{0.02}TiO_3$	SC	1.0	0.98
$NdTiO_3$	SC	0.4	1.00
$Y_{0.2}Ba_{0.8}TiO_{2.85}$	M-SC	0.05	0.50
$Y_{0.33}Ba_{0.67}TiO_{2.9}$	M	0.002	0.50
$Y_{0.4}Ba_{0.6}TiO_{2.9}$	M	0.005	0.53

Transport Properties. Four-probe resistivity measurements were performed on irregularly shaped arc-melted pellets of selected $R_xBa_{1-x}TiO_{3-\delta}$ phases. Due to the difficulties associated with making contact with the bulk phase through the exterior oxide skins, the samples were masked, the contact surfaces cleaned by argon ion milling, and ca. 300–500 Å of Ti and Au was sequentially sputtered onto the contact surfaces prior to attaching the leads with silver paste. The sample resistivities were measured between room temperature and 4 K. Approximations of the sample resistivities were made at room temperature (Table III), but precise determination of the resistivities was precluded due to the irregular shapes of the samples. The data are summarized in Table III, and representative plots of R/R_{300} versus T are given in Figure 6.

The $R_xBa_{1-x}TiO_{3-\delta}$ series where R = Y, Nd, and La all have metallic regions primarily associated with the cubic domains of the corresponding solid solutions. The approximated resistivities of the metallic samples are between 10^{-2} and 10^{-4} Ω·cm, which is similar to many metallic copper oxides[11] and other poorly conducting metallic oxides.[12] The yttrium series shows metallic behavior from

(9) (a) Saltydova, V. A.; Mel'nikova, O. V.; Leonova, N. V.; Fedorov, N. F. *Russ. J. Inorg. Chem.* **1985**, *30* (1), 105. (b) Razgon, E. S.; Gens, A. M.; Varfolomeev, M. B.; Korovin, S. S.; Kostomarov, V. S. *Russ. J. Inorg. Chem.* **1980**, *25* (6), 945.

(10) (a) Kestigan, M.; Ward, R. *J. Am. Chem. Soc.* **1954**, *76*, 6027. (b) Bertaut, E. F.; Forrat, F. *J. Phys. Radium.* **1956**, *17*, 129. (c) Holzapfel, H.; Sieler, J. *Z. Anorg. Allg. Chem.* **1966**, *343*, 174. (d) Ganguly, P.; Parkash, O.; Rao, C. N. R. *Phys. Status Solidi A* **1976**, *36*, 669.

(11) (a) Chien, T. R.; Wang, Z. Z.; Ong, N. P. *Phys. Rev. Lett.* **1991**, *67*, 2088. (b) Gurvitch, M.; Fiory, A. T. *Phys. Rev. Lett.* **1987**, *59*, 1337.

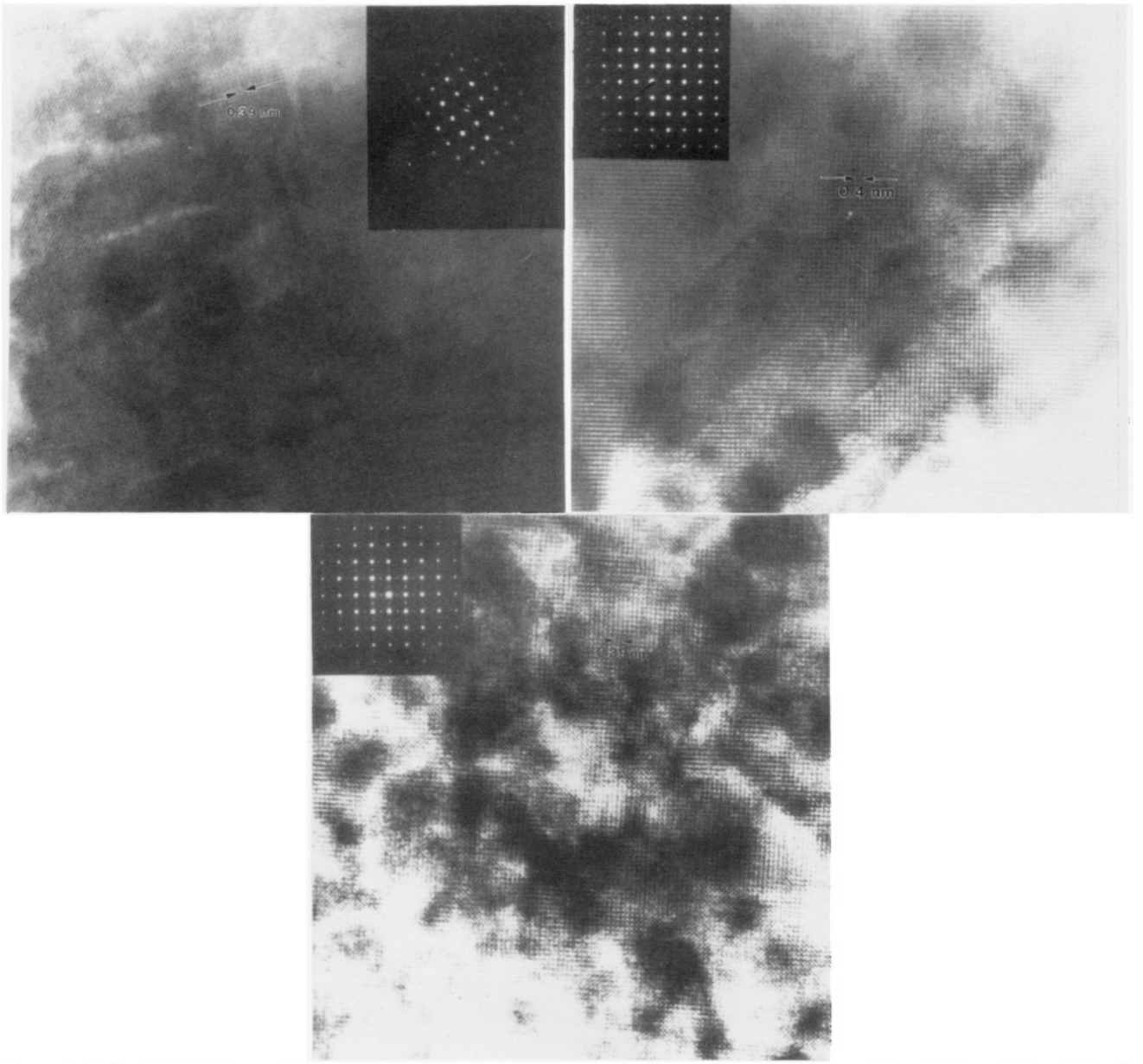

Figure 5. (a, top) HREM image ((100) zone axis) of $Y_{0.33}Ba_{0.67}TiO_{2.9}$ showing the regular ~3.9-Å perovskite cell. The electron diffraction pattern (inset) shows the absence of superstructure reflections: (b, middle) HREM image ((100) zone axis) and electron diffraction pattern (inset) of cubic $La_{0.70}Ba_{0.20}TiO_{2.9}$ showing the regular ~4.0-Å perovskite cell. (c, bottom) HREM image ((001) zone axis) and electron diffraction pattern (inset) of orthorhombic $La_{0.70}Ba_{0.20}TiO_{2.9}$. The ~4.0-Å perovskite subcell is clearly evident. The camera length is the same for all diffraction patterns.

$x = 0.2$ ($\delta = 0.15$) through the limit of the solid solution range at $x = 0.4$ ($\delta = 0.10$). A temperature-induced metal-to-semiconductor transition was observed at 120 K for the $x = 0.2$ phase (Figure 6c). The metallic region for the neodymium series extends from $x > 0.28$ through the biphasic region and again becomes semiconducting at $x > 0.9$. Ceramic samples of $NdTiO_3$ were found to be semiconducting with a calculated band gap of 5×10^{-3} eV, which is in reasonable agreement with the 3×10^{-2} eV gap determined from a single-crystal study.[13] The metallic region of the lanthanum series extends from $x > 0.2$ to $x = 1.0$.

Magnetic Studies. The magnetic susceptibilities of the Y, Nd, and La materials were measured between 4 K and room temperature at fields of 1–50 kOe. The $La_xBa_{1-x}TiO_3$ phases showed Pauli-like temperature-independent susceptibilities for $0.33 \leq x \leq 1.0$ which is consistent with the observed metallic behavior and the previous work on $LaTiO_3$.[2] Plots of susceptibility versus temperature for the $x = 0.33$, 0.70, and 0.85 members of the $La_xBa_{1-x}TiO_3$ phases are shown in Figure 7a. The data can be fit by the Curie–Weiss law:

$$\chi = \chi_0 + C/(T - \theta)$$

where χ is the magnetic susceptibility, χ_0 is the temperature-independent susceptibility, C is the Curie constant, and θ is the Weiss constant. The magnitude of the Pauli paramagnetism (χ_{Pauli}) due to the conduction electrons was extracted from the temperature independent χ_0 terms of the susceptibilities according to the following equation:

$$\chi_0 = \chi_{Pauli} + \chi_{Landau} + \chi_{core}$$

where χ_{Landau} is the diamagnetic orbital contribution due to the conduction electrons and χ_{core} is the core diamagnetism.[14] Because the semiconducting $NdTiO_3$ showed

(12) Torrance, J. B.; Lacorro, P.; Asavaroengchai, C.; Metzger, R. M. *J. Solid State Chem.* **1991**, *90*, 168.
(13) MacLean, D. A.; Seto, K.; Greedan, J. E. *J. Solid State Chem.* **1981**, *40*, 241.

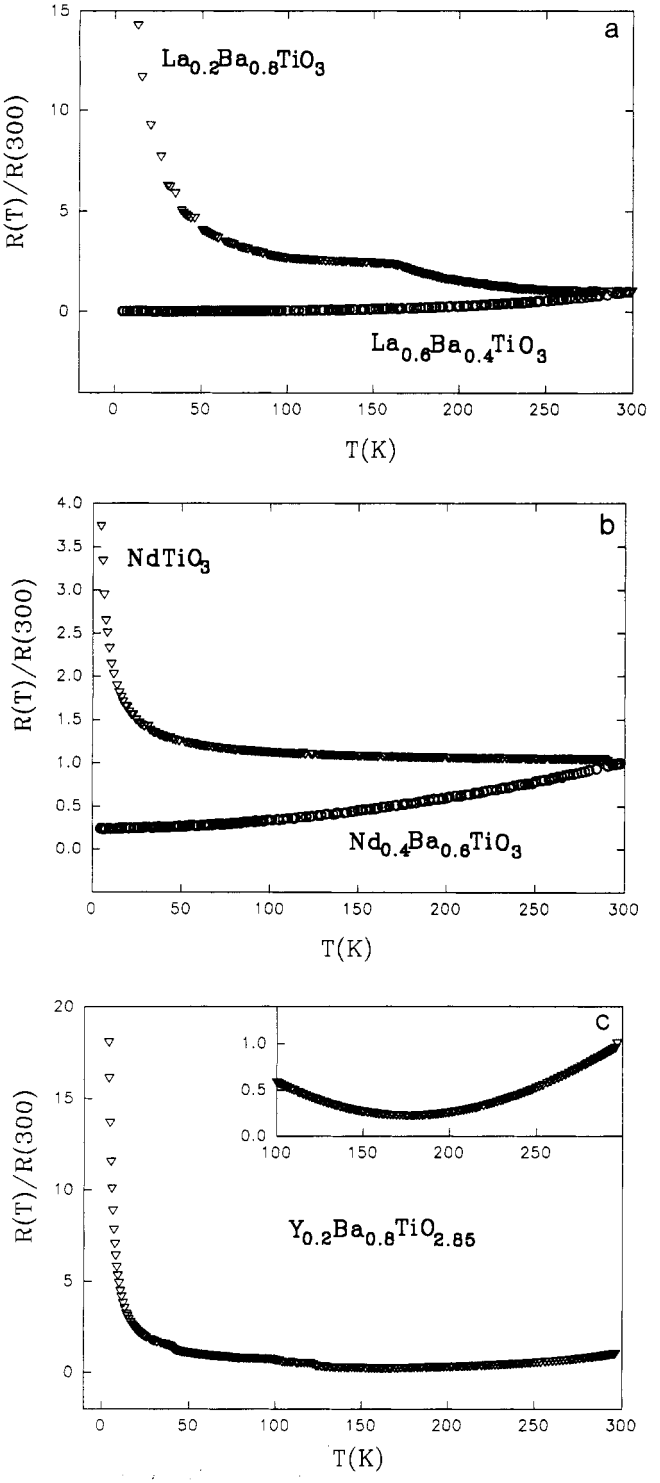

Figure 6. Representative plots of relative resistance (R/R_{300}) versus temperature for (a) the $La_xBa_{1-x}TiO_3$ series, (b) the $Nd_xBa_{1-x}TiO_3$ series, and (c) $Y_{0.2}Ba_{0.8}TiO_{2.85}$. The inset illustrates the metal–semiconductor transition.

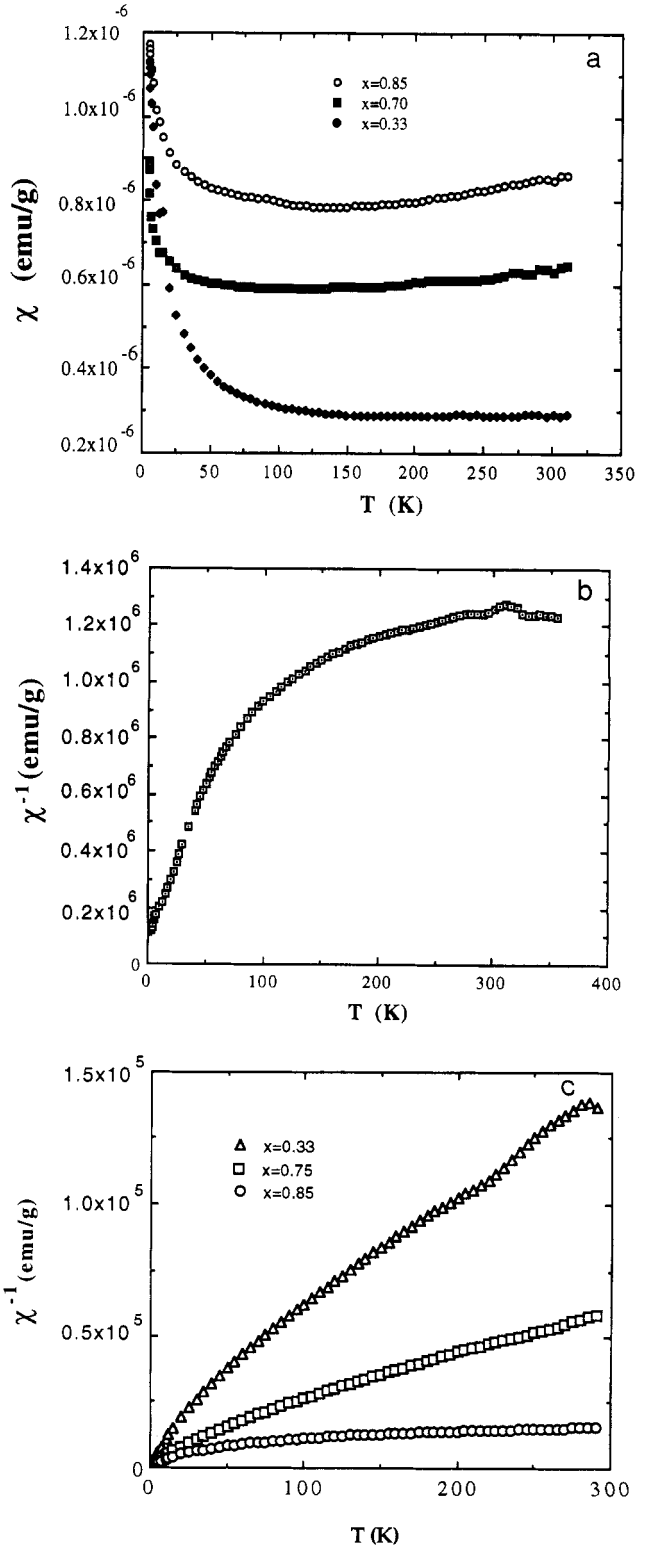

Figure 7. (a) Plots of molar susceptibility versus temperature for three $La_xBa_{1-x-y}TiO_{3-y}$ phases (for $x = 0.33$ and 0.85, $y = 0$; for $x = 0.7$, $y = 0.1$). Data were recorded in a 50-kOe field. (b) Plot of inverse molar susceptibility versus temperature for $Y_{0.33}Ba_{0.57}TiO_{2.9}$. Data were recorded in a 50-kOe field. (c) Representative plots of inverse molar susceptibility versus temperature for the $Nd_xBa_{1-x}TiO_3$ phases. Data were recorded in a 1-kOe field.

no temperature-independent susceptibility, we assumed that the Van Vleck contribution to the χ_0 term was negligible and was not taken into account in our analyses. The core diamagnetism was estimated from literature values.[15] With the assumption that the effective mass of the conduction electrons (m^*) is equal to the mass of the free electron (m), the χ_{Landau} term

$$\chi_{Landau} = -\frac{1}{3}(m/m^*)^2\chi_{Pauli}$$

can be approximated as

(14) (a) White, R. M. *Quantum Theory of Magnetism*; McGraw-Hill: New York, 1970; p 86. (b) Peng, J. L.; Klavins, P.; Shelton, R. N.; Radousky, H. B.; Hahn, P. A.; Bernardez, L.; Costantino, M. *Phys. Rev. B* **1989**, *39*, 9074.

(15) Selwood, P. W. *Magnetochemistry*, 2nd ed.; Interscience: New York, 1970; p 78.

$$\chi_{Landau} = -\frac{1}{3}\chi_{Pauli}$$

The Pauli components can then be calculated from the relationship[14]

$$\chi_{Pauli} = \frac{3}{2}(\chi_0 - \chi_{core})$$

The data are summarized in Table IV. The magnitude of the Pauli susceptibilities in both the La and Y series decrease with decreasing carrier concentration (Ti^{3+} concentration) as expected. In addition, the yttrium samples displayed unusual but reproducible anomalies near room temperature (Figure 7b). Comparison of the χ_{Pauli} values for $Y_{0.33}Ba_{0.67}TiO_{2.9}$ and $La_{0.33}Ba_{0.67}TiO_3$ show a higher susceptibility for the Y phase which is consistent with the differences in Ti oxidation states due to the oxygen vacancies.

The susceptibilities of the $Nd_xBa_{1-x}TiO_3$ phases are dominated by the magnetic Nd^{3+} ions ($4f^3$) and display Curie–Weiss paramegnetism over large temperature ranges. Assuming that the Ti based electrons only contribute to the χ_0 term for the metallic samples, the effective magnetic moment per Nd^{3+} ion, μ, can be calculated from the Curie constant, C, according to the following equation:

$$C = \mu^2 g^2 N/3k$$

where g = the Lande' factor, N is the number of Nd^{3+} atoms per gram, and k is Boltzman's constant. The effective magnetic moments, Curie constants, Weiss constants, and Pauli susceptibilities are listed in Table V. The data show an essentially constant μ_{eff} of ca. 3.3 μ_B when $x \leq 0.9$, which is slightly less than the free ion moment of 3.62 μ_B for Nd^{3+}.

Low-field susceptibilities (10 Oe) of all $R_xBa_{1-x}TiO_{3-\delta}$ samples at 4 K showed no diamagnetic signals, that would be suggestive of superconductivity.

Discussion

Homogeneous solid solutions of formula $R_xBa_{1-x}TiO_{3-\delta}$ where $0 \leq x \leq 1$ were observed for R = La and Nd with the exception of the two-phase region at $0.70 \leq x \leq 0.85$ for R = Nd and $0.60 \leq x \leq 0.90$ for R = La resulting from apparent first order cubic-to-orthorhombic phase transitions. Conversely only small amounts of R^{3+} for Ba^{2+} substitution was observed at low values of x for the smaller trivalent ions Gd^{3+}, Er^{3+}, and Y^{3+} and virtually no Ba^{2+} for R^{3+} replacement was observed at high values of x. This behavior most likely results from the increasing A site size disparity between Ba^{2+} and the R^{3+} ions as one progresses from La^{3+} to Y^{3+}. A similar situation was observed in the $(Na,Li)_2SiO_3$ solid solutions in which more than 50% of the Na^+ ions in Na_2SiO_3 were replaced by the smaller Li^+ ions but only ca. 10% of the Li^+ ions in Li_2SiO_3 could be replaced by the larger Na^+ ions.[16]

The compositionally dependent tetragonal ($P4mm$)-to-cubic ($Pm3m$) phase transition at small values of x in the $R_xBa_{1-x}TiO_{3-\delta}$ series appears to be continuous and is a symmetry-allowed second-order process according to the Landau theory.[17] The cubic ($Pm3m$)-to-orthorhombic ($Pbnm$) phase transition appears to be discontinuous (first order) and may involve tetragonal intermediates[18] with $P4/mbm$ symmetry; however, we were not able to detect such species. Sunstrom and Kauzlarich have suggested that the transition from orthorhombic ($Pbnm$)-to-cubic ($Pm3m$) in $La_xBa_{1-x}TiO_3$ is continuous and involves an

Table IV. Pauli Susceptibilities and Number of d Electrons for the $R_xBa_{1-x}TiO_{3-\delta}$ Phases Where R = Y, La

sample	χ_{Pauli}, emu/mol	d electrons per formula unit
$La_{0.33}Ba_{0.67}TiO_3$	2.08×10^{-4}	0.33
$La_{0.7}Ba_{0.2}TiO_{2.9}$	3.05×10^{-4}	0.70
$La_{0.85}Ba_{0.15}TiO_3$	3.99×10^{-4}	0.85
$Y_{0.2}Ba_{0.8}TiO_{2.85}$	3.14×10^{-4}	0.50
$Y_{0.33}Ba_{0.67}TiO_{2.9}$	3.42×10^{-4}	0.53
$Y_{0.4}Ba_{0.6}TiO_{2.9}$	3.83×10^{-4}	0.60

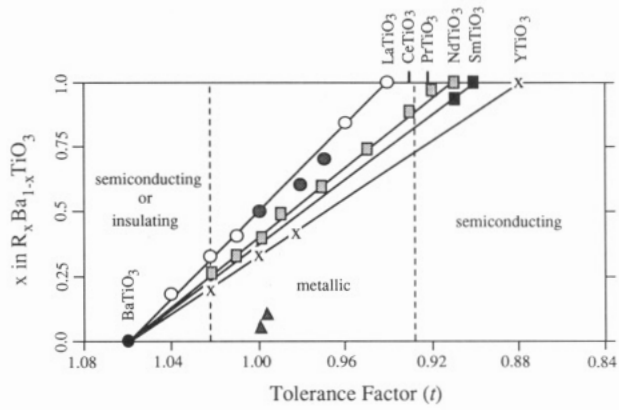

Figure 8. Transport sorting diagram showing the metallic and two semiconducting regions of the $R_xBa_{1-x}TiO_{3-\delta}$ series. The Y series is represented by X, the Sm series by black squares, the Nd series by white squares, and the La series by circles. The shaded circles denote the BaO deficient phases. The shaded triangles represent the x = 0.05 and 0.10 members of the $La_xSr_{1-x}TiO_{3-\delta}$ series.[21] Data for $SmTiO_3$ and $Sm_{0.95}Ba_{0.05}TiO_3$ were taken from refs 1 and 26, respectively.

Ibmm intermediate.[7d] A proper analysis of this phase transition will require a high-temperature X-ray diffraction study in that our compositions as prepared do not represent the high-temperature regions of the equilibrium phase diagram. The biphasic nature of some compositions may result from a slow quench from high-temperature single phases. The cell parameter changes in the $R_xBa_{1-x}TiO_{3-\delta}$ systems (R = Y, Er, Gd) are suggestive of nonequilibrium conditions.

Negative departures from Vegard's law are observed in the cubic region of the $La_xBa_{1-x}TiO_3$ system (see Figure 2b); however, no departures could be detected throughout the entire cubic domain of the $Nd_xBa_{1-x}TiO_3$ solid solution. The BaO deficiencies observed in the single-phase samples of the lanthanum system may be responsible for the nonlinear relationship between x and a. The absence of BaO deficiencies in the Nd systems supports this hypothesis.

X-ray diffraction and HREM studies show that the cubic $Pm3m$ structure persists throughout most of the $R_xBa_{1-x}TiO_{3-\delta}$ solid solutions without the formation of superstructures or ordered microdomain states as have been observed in related $Ca_xLa_{1-x}FeO_{3-y}$ phases.[19] This behavior is somewhat surprising in view of the large size discrepancy between Ba^{2+} and the trivalent ions.

The metallic regions of the solid solutions studied to date correlate quite well with the perovskite tolerance factor t, where

$$t = (r_A + r_O)/\sqrt{2}(r_B + r_O)$$

where r_B and r_A are the six-coordinate $Ti^{3+/4+}$ (B site) radius and the average twelve-coordinate A site radius,

(16) West, A. R. Solid State Chemistry and Its Applications; John Wiley & Sons: New York, 1984; p 360.
(17) Franzen, H. F.; Chen, B.-H. *J. Solid State Chem.* **1990**, *88*, 247.
(18) Wang, Y.; Guyot, F.; Yeganeh-Haeri, A.; Liebermann, R. C. *Science* **1990**, *248*, 468.
(19) Alario-Franco, M. A.; Gonzalez-Calbet, J. M.; Vallet-Regi, M. *J. Solid State Chem.* **1983**, *49*, 219.

Table V. Magnetic Data for the $Nd_xBa_{1-x}TiO_3$ Compounds

sample	Curie const C, emu·K/g	Weiss const θ, K	μ_{eff} Nd^{3+}, μ_B	χ_{Pauli}, emu/mol	d electrons per formula unit
$Nd_{0.28}Ba_{0.72}TiO_3$	1.73×10^{-3}	−38	3.41	4.95×10^{-4}	0.28
$Nd_{0.33}Ba_{0.67}TiO_3$	1.84×10^{-3}	−27	3.22	6.71×10^{-4}	0.33
$Nd_{0.75}Ba_{0.25}TiO_3$	4.75×10^{-3}	−37	3.48	1.03×10^{-3}	0.75
$Nd_{0.85}Ba_{0.15}TiO_3$	4.31×10^{-3}	−9	3.11	1.81×10^{-2}	0.85
$Nd_{0.90}Ba_{0.10}TiO_3$	5.59×10^{-3}	−20.4	3.45	1.36×10^{-3}	0.90
$NdTiO_3$[a]	7.37×10^{-3}	−35	2.04		1.00

[a] Data from ref 13.

respectively.[20] Provided that there are conduction electrons present, it appears that metallic behavior is observed when t is in the range $0.93 \leq t \leq 1.02$ with semiconducting behavior on either side of this range (see Figure 8). Greedan has explained the trends in the $RTiO_3$ series as resulting from an increase in localization (narrower Ti 3d bandwidth) due to the increase in orthorhombic distortion from La to Lu.[2] In our systems, substitution of the large Ba^{2+} ion for the smaller rare-earth ions decreases the orthorhombic distortion (by increasing t) and initiates metallic conductivity (e.g., the Nd–Ba–Ti–O system). In addition, there appears to be a maximum t value of ca. 1.02 above which semiconducting or insulating behavior is again observed. The carrier concentrations seem to be less important as illustrated by comparing semiconducting $La_{0.2}Ba_{0.8}TiO_3$ (t = 1.04) with metallic $Y_{0.2}Ba_{0.8}TiO_{2.85}$ (t = 1.02) and semiconducting $NdTiO_3$ (t = 0.91) with metallic $LaTiO_3$ (t = 0.94). Moreover, the single-crystal studies on the x = 0.05 and 0.10 members in the $La_xSr_{1-x}TiO_3$ series[21] reveal metallic conductivity which, despite the low carrier concentrations, is consistent with our structural sorting model shown in Figure 8.

It is interesting to compare the metal-to-semiconductor (or insulator) transitions at low values of x in the $R_xBa_{1-x}TiO_{3-\delta}$ series to the superconducting-to-semiconducting transformations observed in the $Tl(Sr_{1-x}Ba_xLa)$-CuO_5 series.[22] Electron localization in the latter phases is ascribed to narrowing of the $x^2 - y^2$ (Cu–O σ^*) bands that results from increasing the Cu–O distances as the larger Ba^{2+} is substituted for the smaller Sr^{2+}. At $x > 0.3$, the $x^2 - y^2$ band drops below the Tl 6s band and superconductivity (and metallic conductivity) is destroyed. In the $R_xBa_{1-x}TiO_{3-\delta}$ series, the conduction band is a t_{2g} Ti–O π^* type which has much weaker M–O overlap than the σ^* bands in the copper systems. However, in the titanium systems, a similar type of band narrowing must occur as the Ti–O bond distances increase due to increasing Ba^{2+} substitution. As the Ti(3d)–O(2p) π-overlap decreases with increasing Ti–O distance, the transfer energy, b, decreases to the extent that metallic conductivity is destroyed. In terms of Goodenough's model,[23,24] $b_\pi < b_m$[25] and localized behavior is observed. The value of b_π is affected by not only the Ti–O distance but also the diffusivity of the Ti-3d orbitals which is influenced by the basicity of the rare-earth ions. Therefore, one would not expect to observe a metal–insulator transition at a fixed Ti–O distance in each $R_xBa_{1-x}TiO_{3-\delta}$ series. The tolerance factors used to predict the metallic cutoff in Figure 8 are purely steric in nature and do not take into account the electronic effects of the A-site cations. The fact that $Nd_{0.28}Ba_{0.72}TiO_3$ (t = 1.019, Ti–O = 1.982 (1) Å) is insulating whereas $La_{0.33}Ba_{0.67}TiO_3$ (t = 1.022, Ti-O = 1.988 (1) Å) is metallic is consistent with the electronic differences between Nd^{3+} and La^{3+} where the greater basicity of La^{3+} produces a larger b_π despite the longer Ti–O separation.

The susceptibility of $NdTiO_3$ has been analyzed[13] in terms of contributions from both Nd^{3+} ($4f^3$) and Ti^{3+} ($3d^1$), which is consistent with localized titanium 3d electrons and the observed semiconducting behavior of the compound. By comparison with the isostructural $NdScO_3$ phase [Nd^{3+} ($4f^3$) and Sc^{3+} ($3d^0$)], the Nd^{3+} contribution to the total moment of $NdTiO_3$ was estimated at 2.04 μ_B, which is suppressed from its free ion value of 3.62 μ_B.[13] The suppression was ascribed to crystal field effects. Titanium, on the other hand, is proposed to contribute 1.72 μ_B, which is essentially the spin only value (1.71 μ_B). In contrast, our data suggest that, at $x < 0.9$ in the $Nd_xBa_{1-x}TiO_3$ series, the Nd^{3+} contribution to the observed moment is ca. 3.3 μ_B, which is close to the free ion value (see Table V). It is possible that the Nd^{3+} moment is suppressed with increasing orthorhombic distortion (as x approaches 1.0) to arrive at the 2.04 μ_B value proposed by Greedan.[13]

In summary, the appearance of metallic conductivity correlates quite well with the perovskite tolerance factor and is less sensitive to carrier concentration. At the upper and lower limits of the metallic regions, semiconducting behavior is initiated by localization due to elongated Ti–O interactions (large a) and orthorhombic distortions (small r_A), respectively. Further studies are in progress to test this model.

Acknowledgment. B.E. acknowledges the support of the National Science Foundation (DMR-8913906), the Exxon Education Foundation, the Center for Superconductivity Research and Department of Chemistry, University of Maryland. We are indebted to Prof. Cary Miller for assistance with the sputtering experiments and Dr. Cherie Miller for assistance with the AA experiments. We also thank Professor H. Franzen for helpful insights into the phase transitions.

Registry No. $BaTiO_3$, 12047-27-7; $La_{0.15}Ba_{0.85}TiO_3$, 143075-91-6; $La_{0.2}Ba_{0.8}TiO_3$, 131343-60-7; $La_{0.33}Ba_{0.67}TiO_3$, 131344-55-3; $La_{0.4}Ba_{0.6}TiO_3$, 131343-61-8; $La_{0.5}Ba_{0.4}TiO_{2.9}$, 143075-90-5; $La_{0.6}Ba_{0.3}TiO_{2.9}$, 143075-89-2; $La_{0.7}Ba_{0.2}TiO_{2.9}$, 143075-88-1; $La_{0.85}Ba_{0.15}TiO_3$, 143075-87-0; $La_{0.9}Ba_{0.1}TiO_3$, 143075-86-9; $LaTiO_3$, 12201-04-6; $Nd_{0.1}Ba_{0.9}TiO_3$, 143075-85-8; $Nd_{0.28}Ba_{0.72}TiO_3$, 143075-84-7; $Nd_{0.3}Ba_{0.7}TiO_3$, 143075-83-6; $Nd_{0.33}Ba_{0.67}TiO_3$, 143075-82-5; $Nd_{0.4}Ba_{0.6}TiO_3$, 143075-81-4; $Nd_{0.5}Ba_{0.5}TiO_3$, 143075-80-3; $Nd_{0.6}Ba_{0.4}TiO_3$, 143075-79-0; $Nd_{0.7}Bi_{0.3}TiO_3$, 143075-78-9; $Nd_{0.75}Ba_{0.25}TiO_3$, 143075-77-8; $Nd_{0.85}Ba_{0.15}TiO_3$, 143075-76-7; $Nd_{0.9}Ba_{0.1}TiO_3$, 143075-75-6; $Nd_{0.98}Ba_{0.02}TiO_3$, 143075-74-5; $NdTiO_3$, 12201-77-3; $Gd_{0.2}Ba_{0.8}TiO_3$, 143075-73-4; $Gd_{0.3}Ba_{0.7}TiO_3$, 143075-72-3; $Gd_{0.33}Ba_{0.67}TiO_3$, 143075-71-2; $Gd_{0.4}Ba_{0.6}TiO_3$, 143075-70-1; $Y_{0.2}Ba_{0.8}TiO_{2.85}$, 143075-69-8; $Y_{0.33}Ba_{0.67}TiO_{2.9}$, 143075-68-7; $Y_{0.4}Ba_{0.6}TiO_{2.9}$, 143075-67-6; $Er_{0.1}Ba_{0.9}TiO_3$, 143075-66-5; $Er_{0.3}Ba_{0.7}TiO_3$, 143075-65-4; Nd, 7440-00-8.

(20) Shannon, R. D. *Acta Crystallogr.* **1976**, *A32* 751.
(21) Higuchi, M.; Aizawa, K.; Yamays, K.; Kodaira, K. *J. Solid State Chem.* **1991**, *92*, 573.
(22) Subramanian, M. A.; Whangbo, M. H. *J. Solid State Chem.* **1992**, *49*, 219.
(23) Goodenough, J. B.; Longo, J. M. *Landolt-Bornstein*; Springer-Verlag: Berlin, 1970; Group III/4a, p 129.
(24) Goodenough, J. B. *Prog. Solid State Chem.* **1975**, *5*, 145.
(25) b_π is the π transfer energy and b_m is the critical transfer energy required for metallic conductivity.
(26) Eylem, C. E.; Eichhorn, B. W., results to be published.